Ultrasonics Sonochemistry 17 (2010) 258–265

Contents lists available at ScienceDirect

Ultrasonics Sonochemistry

journal homepage: www.elsevier.com/locate/ultsonch

Modeling the coupling of reaction kinetics and hydrodynamics in a collapsing cavity

Sudib K. Mishra [a,*], P.A. Deymier [b], Krishna Muralidharan [b], G. Frantziskonis [a,b], Sreekanth Pannala [c], Srdjan Simunovic [c]

[a] Dept. of Mechanical and Aerospace Engineering, University of California, Irvine, CA 92697, United States
[b] Dept. of Materials Science and Engineering, University of Arizona, Tucson, AZ 85721, United States
[c] Computer Science and Mathematics Division, Oak Ridge National Laboratory, Oak Ridge, TN 37831, United States

ARTICLE INFO

Article history:
Received 10 April 2009
Accepted 18 May 2009
Available online 22 May 2009

Keywords:
Cavitation
Reaction
Multiphase
Lattice Boltzmann Model
Stochastic

ABSTRACT

We introduce a model of cavitation based on the multiphase Lattice Boltzmann method (LBM) that allows for coupling between the hydrodynamics of a collapsing cavity and supported solute chemical species. We demonstrate that this model can also be coupled to deterministic or stochastic chemical reactions. In a two-species model of chemical reactions (with a major and a minor species), the major difference observed between the deterministic and stochastic reactions takes the form of random fluctuations in concentration of the minor species. We demonstrate that advection associated with the hydrodynamics of a collapsing cavity leads to highly inhomogeneous concentration of solutes. In turn these inhomogeneities in concentration may lead to significant increase in concentration-dependent reaction rates and can result in a local enhancement in the production of minor species.

Published by Elsevier B.V.

1. Introduction

There has been revived interest in the chemical effects of high intensity sound waves, namely sonochemistry, since its discovery decades ago [1]. Sonochemistry does not arise from the direct interaction between sound waves and chemical species but via acoustic cavitation [2]. Cavitation is a nonlinear acoustic effect whereby vaporous or gaseous bubbles form as a consequence of pressure variations associated with an acoustic wave. The collapse of unstable cavities leads to extreme conditions of pressure and temperature as well as complex fluid motion such as high velocity fluid jets near solid surfaces. The high energies associated with these extreme conditions can promote chemical reactions and have also been shown to be useful in the synthesis of a large variety of micro and nanoscale structures composed of organic, inorganic materials and biomaterials [3]. The chemical and physical effects of sound can be divided into homogeneous sonochemistry of liquids, heterogeneous sonochemistry of liquid–liquid or solid–liquid systems, with the field of sonocatalysis encompassing all these categories. A complete theoretical understanding of sonochemical processes is not at hand due to the complexity of the coupled physical and chemical processes involved. For instance, a model of the formation of free radicals driven by cavitation requires that the kinetics of free radical formation be linked to the cavity dynamics [4–6]. Recently, Sharma et al. [7] provided a review of important models that couple cavity dynamics, heat transfer, mass transfer and chemical reactions. While the simplest models assume a uniform cavity interior and thus avoid the solution to Navier–Stokes equations [8], it appears important to account for the coupling between the hydrodynamics of the gas in the bubble and associated chemistry [9].

In this paper, we present a model that approaches the coupling between hydrodynamics and chemistry of a collapsing bubble via an extension of the Lattice Boltzmann method (LBM). While at this initial phase we assume the processes to be isothermal, the model considers several aspects of mass transfer including phase change at vapor/liquid interface, diffusion of dissolved species (i.e. solute) as well as changes in concentration of chemical species due to reactions in the liquid and gas core of the bubble. The newly developed LBM offers several advantages compared to other simpler models of cavity dynamics such as the Rayleigh–Plesset equation [10] or the Keller–Miksis equation [11]. LBM can be applied to arbitrary geometry, complex boundaries and offers significant flexibility such as handling of surface interactions, handling multicomponent systems, domain scalability, and algorithmic parallelizability, which are difficult to invoke through commonly available models based on solutions of the governing differential equations. In our study, the basic modeling of bubble formation and collapse is adopted from the work of Sukop and Or [12]. This approach was shown to correctly reproduce key phenomena necessary for the study of cavitation. In addition, the LBM-based model of the hydrodynamics of cavity collapse can be easily linked to chemical transformations of species supported by the cavitating fluid. In this work, we employ two different models of a prototypical chemical reaction. The first one uses deterministic

* Corresponding author. Tel.: +1 520 904 2530; fax: +1 520 621 2550.
E-mail address: mishras@uci.edu (S.K. Mishra).

1350-4177/$ - see front matter Published by Elsevier B.V.
doi:10.1016/j.ultsonch.2009.05.014

rate equations and represents a mean field approximation of the chemical transformations. It is named as coarse model. The second model of chemical reactions is simulated with the kinetic Monte Carlo (kMC) method which accounts for the stochastic nature of the reactions. This latter model, labeled fine, is more realistic than the mean field one but is more computationally demanding.

From a modeling point of view, we show that the kMC used in conjunction with the LBM provides a more detailed and accurate estimation of the kinetic evolution than that given by the mean field model coupled to the LBM. However, this higher degree of realism impacts only the low concentration chemical species (minor species) and does not add significantly to the overall physics and chemistry of reactive-flow near a collapsing cavity. From a sonochemistry point of view, the LBM model coupled with transport of passive chemical species is able to capture the advection of the species at the liquid–vapor interface of the cavity, leading to large enrichment of the region where the cavity collapses and therefore forming highly inhomogeneous distributions of concentration of the chemical species. The coupling of the LBM model with models of chemical reactions leads to enhanced chemical rates in the enriched regions. More specifically the concentration in the minor species can be increase by up to a factor 3 at the core of the collapse cavity.

We present in some details the LBM method for single-component multiphase flow as well as its implementation to simulating advection of dissolved species in Section 2. Section 2 also presents the linear two-species reaction model used for the reactive-flow simulations. In Section 3, we report results of the simulations for cavity collapse in a single-component multiphase fluid. We build on this model to study the effect of advection during cavity collapse on the spatial distribution of passive chemical species supported by the fluid medium. Finally, the coupling between the hydrodynamics of the collapsing cavity, the advection of chemical species and the deterministic or stochastic chemical reactions is characterized via the results of the complete model of the reactive-flow. Conclusions drawn from this study are discussed in Section 4.

2. Methods and model

2.1. Lattice Boltzmann method (LBM) for single-component multiphase flow

We have chosen LBM [13,14] for simulation the cavitation and bubble collapse because of its efficiency and flexibility to incorporate many complex interactions. It can be used for single-component multiphase system such as water and vapor. While details of the method can be found elsewhere [13,15], we adopt the two-dimensional nine velocity component lattice (D2Q9) with velocities e_a. Here $a = 1,3,5,7$ represents velocities along the axial directions, $a = 2,4,6,8$ represents velocities along the diagonal directions and $a = 9$ corresponds to the particle at rest. The magnitudes of the axial components are 1 (lsu ltu^{-1}), the diagonal ones are $\sqrt{2}$ (lsu ltu^{-1}), where lsu stands for a dimensionless lattice space unit and ltu for a lattice time unit. All quantities are expressed in terms of ltu and lsu, linked to the physical system by the following relations:

$$v = (\tau - 0.5)RT\delta t \tag{1}$$

$$c = \delta_x/\delta_y \tag{2}$$

and

$$c_s^2 = RT = c^2/3 \tag{3}$$

where, v is the kinematic viscosity, τ is the relaxation parameter, R is universal gas constant, T is absolute temperature of the system, c is the speed of light in the lattice determined by the spatial (δ_x) and temporal resolution (δ_t), c_s is the speed of sound in the lattice. With the adopted values of τ, c, c_s, we can adjust the geometric physical parameters $\delta x, \delta y, \delta t$ (space/time resolutions) and fluid viscosity (v) to represent a real system. With this configuration, a single particle distribution function f_a will have nine distinct bins. Such a distribution function can visualized as direction-specific fluid densities. The macroscopic density can therefore be summed up from these directional densities.

$$\rho = \sum_{a=1}^{9} f_a \tag{4}$$

The macroscopic velocity u is the average of the microscopic velocities e_a weighted by the directional densities f_a

$$u = \frac{1}{\rho}\sum_{a=1}^{9} f_a e_a \tag{5}$$

This allows passing of the discrete microscopic velocities of the LBM lattice to the macroscopic fluid continuum.

The next operations are streaming/propagation and collision of the fluid particles through distribution functions. The Bhatnagar–Gross–Krook (BGK) approximation is used for collision. Streaming and collision to attain relaxation toward local equilibrium are given by

$$f_a(x + e_a\Delta t, t + \Delta t) = f_a(x,t) - \frac{(f_a(x,t) - f_a^{eq}(x,t))}{\tau} \tag{6}$$

The first part of the above equation represents the streaming from one node to its neighbor and the second term is due to collision. Collision can be thought of as relaxation toward local equilibrium and for the D2Q9 lattice the equilibrium distribution function f_a^{eq} is defined as

$$f_a^{eq}(x) = w_a\rho(x)\left[1 + 3\frac{e_a u}{c^2} + \frac{9}{2}\frac{(e_a u)^2}{c^4} - \frac{3}{2}\frac{u^2}{c^2}\right] \tag{7}$$

where, the weights w_a are $\frac{4}{9}$ for the rest particles $(a = 9)$, $\frac{1}{9}$ for axial directions $a = 1,3,5,7$ and $\frac{1}{36}$ for $a = 2,4,6,8$ for diagonal directions. c is the speed of sound on the lattice, taken as 1/3 (lsu ltu^{-1}).

For multiphase fluid flow, interactions between fluid particles are incorporated. Nearest neighbor attractive interactions is able to simulate the basic phenomena of single-component multiphase fluids. In D2Q9 lattice an attractive force F among nearest neighbor fluid particles is expressed as

$$F(x,t) = -G\psi(x,t)\sum_{a=1}^{9} w_a\psi(x + e_a\Delta t, t)e_a \tag{8}$$

where G denotes the interaction strength and ψ the interaction potential. Whereas alternative forms of potential functions are available, the one used herein is given by

$$\psi(\rho) = \psi_0 \exp(-\frac{\rho_0}{\rho}) \tag{9}$$

where ψ_0 and ρ_0 are constants [16,17]. $G < 0$ gives the attraction between the particles and the force is stronger when the density is higher (leading to surface tension at a vapor–liquid interface).

The force term given by Eq. (8) is incorporated in the LBM simulation by adding a velocity terms to the existing lattice velocity, following the Newton's equation of motion:

$$F(x,t) = \rho(x,t)\frac{d\Delta u_{lr}}{dt} \tag{10}$$

where, $\rho(x,t)$ is the density of fluid at the lattice and Δu_{lr} is the added velocity term due to long range interactions. Recalling the

fact that the relaxation time τ is the elementary time of collisions, we can rearrange Eq. (10) as

$$\Delta u_{lr}(x,t) = \tau F(x,t)/\rho(x,t) \tag{11}$$

and then the total velocity becomes

$$u_{eq} = u + \Delta u_{lr} \tag{12}$$

This resultant velocity (u_{eq}) is used in the computation of the equilibrium probability distribution function $f_a^{eq}(x,t)$, shown in Eq. (7). The effect of the strength parameter G on the equation of state of a LBM fluid is contrasted against that of water in Fig. 1.

In our model we consider the presence of hydrodynamically passive solute chemical species. These are species that are supported and are solely transported by the cavitating base fluid [14,19]. Two common modes of transport are diffusion (or mass transport) and advection (or momentum transfer). In addition to the basic phenomena of cavitation and bubble collapse, the LBM has ability to simulate transport of species through advection and diffusion. This transport is simulated by a second distribution f_σ called the solute distribution where σ represents the passive species. The solute distribution takes on a form similar to that of the supporting fluid distribution function but involves terms up to first-order velocity components. The solute distribution is given by:

$$f_{\sigma,a}^{eq} = w_a \rho_\sigma (1 + 3 e_a \cdot u) \tag{13}$$

where, w_a are the same weight coefficients associated with particular directions of the lattice (diagonal and axial), and ρ_σ is the density of the specie σ written as

$$\rho_\sigma = \sum_{a=1}^{9} f_{\sigma,a} \tag{14}$$

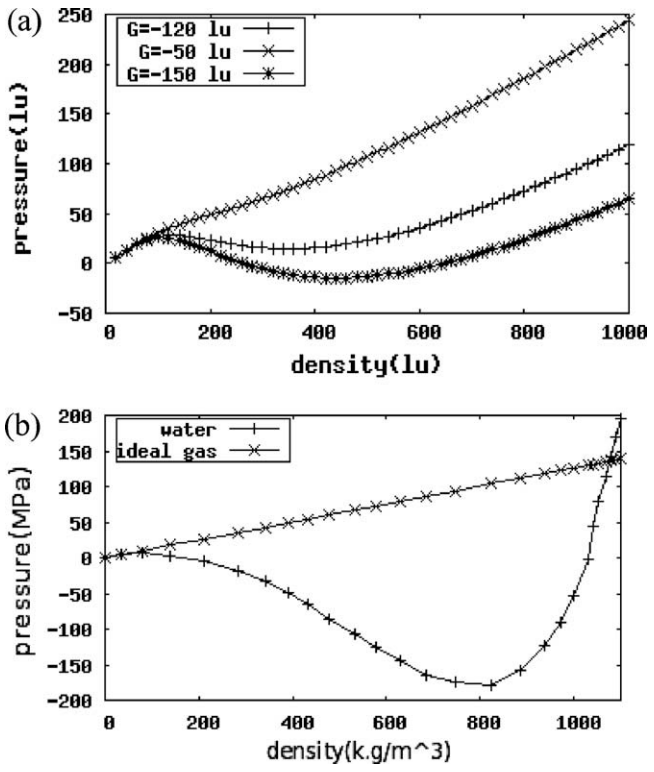

Fig. 1. (a) The pressure–density ($P-\rho$) relationship of the LBM fluid for various levels of strength of potential (G). Both density and pressure are expressed in lattice units (lu); (b) The ($P-\rho$) relation for water [18]. The correspondence between lattice and physical units is derived from these plots.

In Eq. (13), u is the velocity of the fluid. Eq. (14) is analogous to the fluid density given in Eq. (4). The diffusion coefficient of the passive species is expressed in terms of a relaxation parameter (τ_σ)

$$D_\sigma = \frac{1}{3}\left(\tau_\sigma - \frac{1}{2}\right) \tag{15}$$

The same steps of propagation/streaming, equilibration and collision are applicable to the passive species.

2.2. Chemical reactions

In order to investigate the coupling between the hydrodynamics of a collapsing cavity and transformation of chemical species dispersed in the cavitating fluid, we consider for the sake of simplicity the case of a bi-molecular reversible chemical reaction. Since our focus is on hydrodynamics/chemical reactivity coupling, we assume that the cavity collapses isothermally and we leave the thermal effects on the chemical reactions to a subsequent study. In our model, the chemical reactions are simulated by two different techniques. The first technique solves the ordinary differential equations governing the chemical kinetics by finite differences using standard numerical methods. The second model uses the probability of occurrence of a reaction event and relies on the kinetic Monte Carlo (kMC) method to march the reactions in time. The former model is termed as "coarse" while the latter is termed as "fine" model. The term fine refers to the ability of that model to resolve the reaction kinetics over much finer temporal and spatial scales that the coarse model allows.

We consider bi-molecular reversible reactions $A \overset{k_f}{\rightarrow} B$ and $B \overset{k_b}{\rightarrow} A$, with linear reaction kinetics:

$$\frac{d}{dt}\begin{Bmatrix} A \\ B \end{Bmatrix} = \begin{bmatrix} -k_f & k_b \\ k_f & -k_b \end{bmatrix} \begin{Bmatrix} A \\ B \end{Bmatrix} \tag{16}$$

where, A, B are chemical species considered and k_f and k_b are respectively forward and backward reaction rates. The forward (k_f) and backward reaction rates (k_b) are taken as $k_f = 0.25$ $k_b = 0.125$ ltu^{-1}, respectively. In the coarse model, this set of equations is solved numerically using any of the standard technique like Euler's technique or more accurately using higher order Runge–Kutta scheme. In the fine model, one uses the probability of occurrence of a reaction event expressed as [20]

$$P(R_i) = 1 - \exp(-k_i[S_i]\Delta t) \tag{17}$$

where, P is the probability of occurrence of reaction R_i, k_i is the reaction rate constant, $[S_i]$ is the concentration of the species and Δt is the time demand for the i-th reaction. On inversion the reaction time demands for the forward and reverse reactions are expressed as

$$\Delta t_f = \frac{1}{k_f[A]} \ln\left(\frac{1}{1-R_1}\right) \text{ and } \Delta t_b = \frac{1}{k_b[B]} \ln\left(\frac{1}{1-R_2}\right) \tag{18}$$

The kMC numerical procedure at any lattice node involves picking two independent uniform random numbers between 0 and 1, R_1, R_2 and obtain two time demands for forward and backward reactions. The direction of the reaction is then chosen according to the shortest time demand with a time step $\Delta t = \min\{\Delta t_f, \Delta t_b\}$. Depending on these time demands the species concentrations are updated as

$$\text{for } \Delta t_f \leqslant \Delta t_b \begin{cases} [A] = [A] - 1 \\ [B] = [B] + 1 \end{cases} \text{ and for } \Delta t_b \leqslant \Delta t_f \begin{cases} [A] = [A] + 1 \\ [B] = [B] - 1 \end{cases} \tag{19}$$

It is worth noting that the integration of the deterministic rate equations are much less computationally intensive than the kMC ones, and provide an approximate mean field solution for the

underlying kinetics. The kMC is a stochastic model and captures the details and uncertainties involved in chemical reactions and thus provide a more realistic representation of the underlying kinetics. However owing to the calculation of time demand for individual lattice sites the kMC method is much more computationally exhorbitant.

2.3. Coupling the LBM to the reaction kinetics

We now consider the coupled system involving the collapse of a cavity in the supporting fluid, the reaction kinetics and the diffusion and convection of the chemical species. The species follow the steps of the passive transport within the LBM framework and the reactions take place right after the propagation/streaming steps. The deterministic mean field reaction equations can be synchronized with the LBM time step (within the Courant limits for stability of the algorithm). In contrast, the kMC characteristic time scales are substantially smaller than the LBM time scale. This means many kMC steps need to be accommodated between two successive LBM steps. The kMC operations are performed right after the propagation/streaming step of the LBM simulation. Many such kMC steps in between the LBM time steps make this model quite computationally intensive, yet it captures subtle features of the kinetics.

3. Results and discussion

3.1. Cavity collapse in absence of reactive species

Here we verify the ability of the LBM to model the formation of a cavity as well as the dynamics of a collapsing cavity. We first consider a square domain of liquid 201×201 lattice units. Conditions of outward-going velocities are imposed on the top and bottom boundaries of the domain to decrease the density and bring the liquid into the region of density instability where the liquid coexists with the vapor state, thus forming the initial cavity (see Fig. 2a). The initial cavity possesses a slightly oblong shape to the unidirectional nature of the velocity field used to create it. The domain is then subjected to a uniform hydrostatic state of pressure which is maintained constant at the boundaries of the domain. The pressure is large enough to ensure the cavity progressive collapse. Fig. 2a–d illustrates the time evolution of the fluid density as the cavity collapses under pressure. The slight deviation from a perfect circular shape in the density maps is due to the slightly acicular initial cavity. The subsequent collapse will therefore also differ slightly from a perfect circle. The concentric rings of varying density surrounding the collapsed cavity result from the propagation of an outward high pressure front that forms during the cavity collapse. The evolution of the pressure field throughout the domain is shown in Fig. 3.

The dynamics of the collapse can be better visualized from the time histories of the density and/or pressure at some specific locations within the simulated domain, shown in Fig. 4. All these locations are within the initial cavity. The rapid increase in density at time 20 ltu for the point p5 (most outward location) is indicative of the passage of the liquid–vapor interface due to the collapsing cavity. Similar transitions are occurring successively at points p4, p2, and p3 in order of radial distance from the center of the cavity. The center location (point p1) exhibits a very large increase in density and pressure $\sim$85 ltu through the simulation. These increases correspond to the complete collapse of the cavity that is followed by the propagation of a pressure wave that reaches points p3, p2, p4 and p5 at successive times. The passage of the pressure wave is seen as a sharp increase in pressure accompanied by a significant increase in the density of the liquid.

3.2. Transport of passive species by collapsing cavity in absence of chemical reactivity

Fig. 5 shows the transport of passive chemical species by advection associated with the bubble dynamics. The non-reactive species A and B concentrate at the liquid–vapor interface in response to the hydrodynamics of the collapse. The enrichment of the liquid–vapor interface is not due to surface tension effect as the species A and B are totally passive and do not interact with the supporting fluid but through its velocity field via advection. Here the rate of accumulation of species A and B via advection exceeds the rate of diffusion. The concentration of the species-enriched region also depends on the viscosity and diffusivity of the species. The viscosity of A is much lower than B, which causes relatively higher maximum concentration of A compared to B at the bubble periphery. We see from Fig. 5 that at a time of 60 ltu steps (20 ltu before the complete collapse of the cavity) the maximum concentration of A around the ring is almost $7\times$ the initial concentration whereas it is only $\sim 5\times$ for species B. Furthermore the width of the enriched region is larger for the specie B than for A dues to the higher diffusivity of B.

One can understand the enrichment with the following simple argument. In some interval of time dt, the liquid–vapor interface located at some radial distance r moves inward by a radial amount $-dr$. The passive species on the vapor side of the moving liquid–vapor interface within the shell of radius r and thickness dr gain momentum by advection and accumulate in the shell of radius $r - dr$ crowding the existing species leading to accumulation. On the liquid side of the interface the reverse mechanism occurs leading to depletion. The amount of accumulation or depletion is determined by the relative relaxation times for diffusion (i.e. homogeneization of the species) and the supporting fluid velocity due to the collapsing bubble. In the case of two passive species, A and B, in the supporting fluid, the enrichment factor at any time

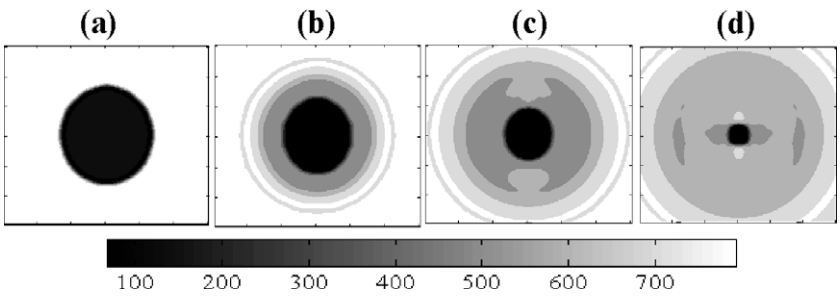

Fig. 2. Progressive collapse of the bubble illustrated in terms of density maps. (a) Cavity at a very early time of 5 ltu, (b)–(d) density maps at times of 25, 50, and 75 ltu, respectively. The gray scale images represent the maximum density as white (85 μ lu^{-2}) and the vapor density inside the cavity as black (800 μ lu^{-2}) where mu stands for mass units.

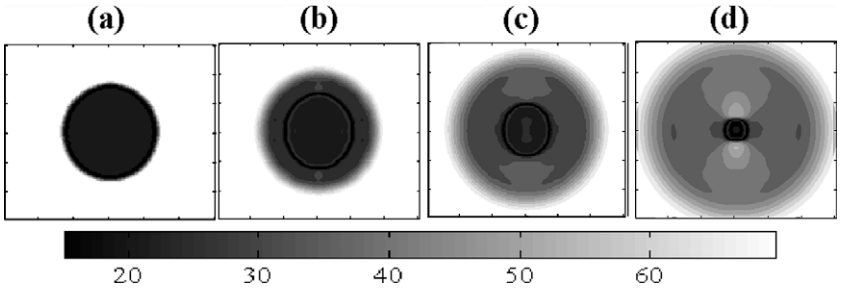

Fig. 3. The pressure field around the collapsing bubble as several times (a) 5, (b) 25, (c) 50, and (d) 75 ltu.

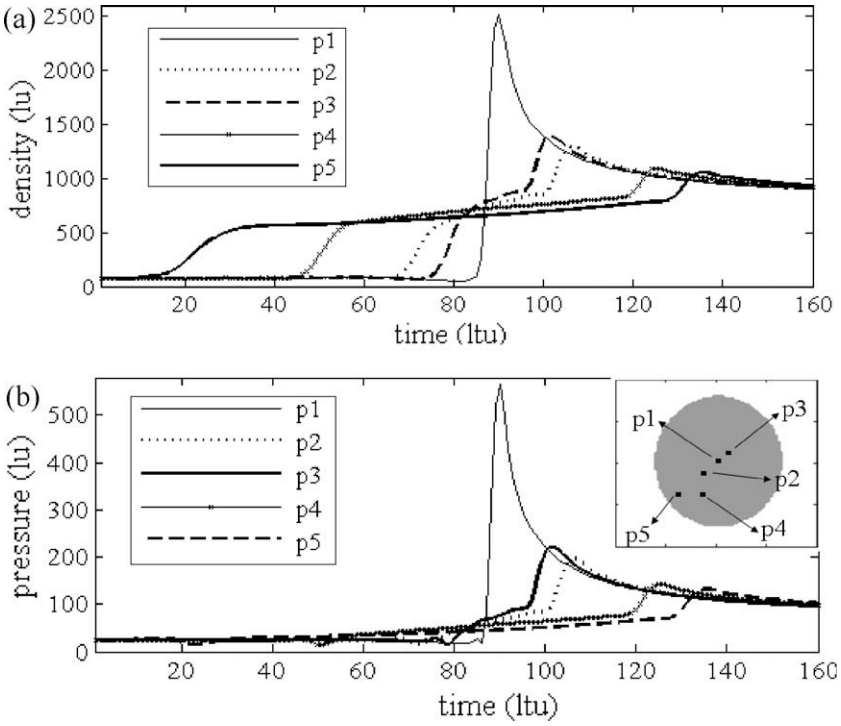

Fig. 4. Time evolution of: (a) density and (b) pressure at several locations within the initial cavity. The locations p1 through p5 are illustrated in the inset of (b). The two-dimensional coordinates of these points in the simulated domain are p1 = (101,101), p2 = (95,95), p3 = (105,105), p4 = (85,95), p5 = (85,85), respectively.

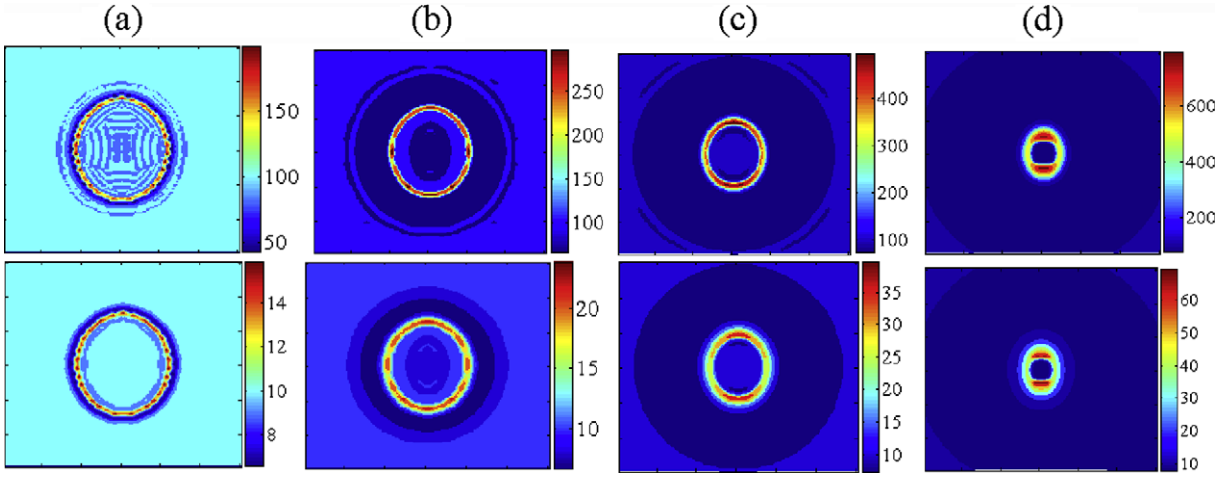

Fig. 5. The distribution of concentration of species A (top row) and B (bottom row) inside the simulated domain after (a) 5, (b) 20, (c) 40, and (d) 60 ltu steps. The species are not chemically reactive. Note the variation in the concentration scale as time evolves indicating continued enrichment at the moving liquid-vapor interface. The initial concentration was uniform and equal to 100 A and 10 B.

and location will be the same if the diffusion coefficients for A and B are identical. However, differences in diffusion constants will lead to locally varying enrichment or depletion ratios. The coupling between the passive species A and B and the flow of fluid associated with the cavity collapse results in an inhomogeneous distribution of these species while still maintaining their overall composition in the simulation domain does not vary.

3.3. Reactive-flow of a collapsing cavity

Here, we combine the hydrodynamics of a collapsing cavity with the advection of supported chemical species A and B as well as the kinetics of the chemical reactions. The initial composition is uniform throughout the simulation domains and set at 100 and 10 for the major species A and the minor species B, respectively. Fig. 6 reports color contour maps of the distribution of the B species in the simulation domain as the cavity collapses for the deterministic reaction model ("coarse") model and the stochastic reaction model ("fine") model. The overall behavior of the reactive species in terms of transport and reaction is very similar for both models as well as both A and B species. Advection leads to concentric accumulation and depletion rings at the liquid/vapor interface as was shown in the previous section. The primary difference between the coarse and the fine models is essentially seen in the maps of the concentration of the minor species B (Fig. 6) where spatially localized fluctuations form due to the stochastic nature of the kMC reactions. However, aside from this difference the two models behave in an analogous way. Note that as the cavity collapses it concentrates the supported species and after the cavity has completely collapsed it left a small enriched region in A and B. The concentration dependency of the chemical reactions given by Eq. (16) will therefore lead to locally enhanced reaction rates. Indeed, the effect of chemical reactivity is quantified in Fig. 7 by comparing the concentration profiles across the simulation domain for the fine model and the model in absence of chemical reactions at several times. In the initial stages of the collapse the enrichment and depletion in A and B at the cavity surface are insufficient to lead to significant difference in concentrations due to chemical reactivity (Fig. 7a). In this figure, one sees, however, the local fluctuations due to the stochastic nature of the chemical reaction model. As time proceeds (50 ltu steps) toward complete collapse, the changes in local concentrations are sufficiently large for the effect of chemical reactions to be seen (Fig. 7b).

We note a time lag in the advancement of the A-enriched ring compared to the simulation without reaction. This lag is associated with the rapid transformation of A into B at the highest A concentration. This transformation leads to a ring of increased B concentration that also lags behind the B ring for the simulation without reactions. At a time of 100 ltu steps (Fig. 7c), the cavity has already completely collapsed and a pressure wave is propagating outward. The time to complete collapse is ~85 ltu steps. In absence of chemical reactivity, we observe the large enrichment in A and B in the centrally located region followed by diffusion. The propagation of the pressure waves leads to advection of the species and the

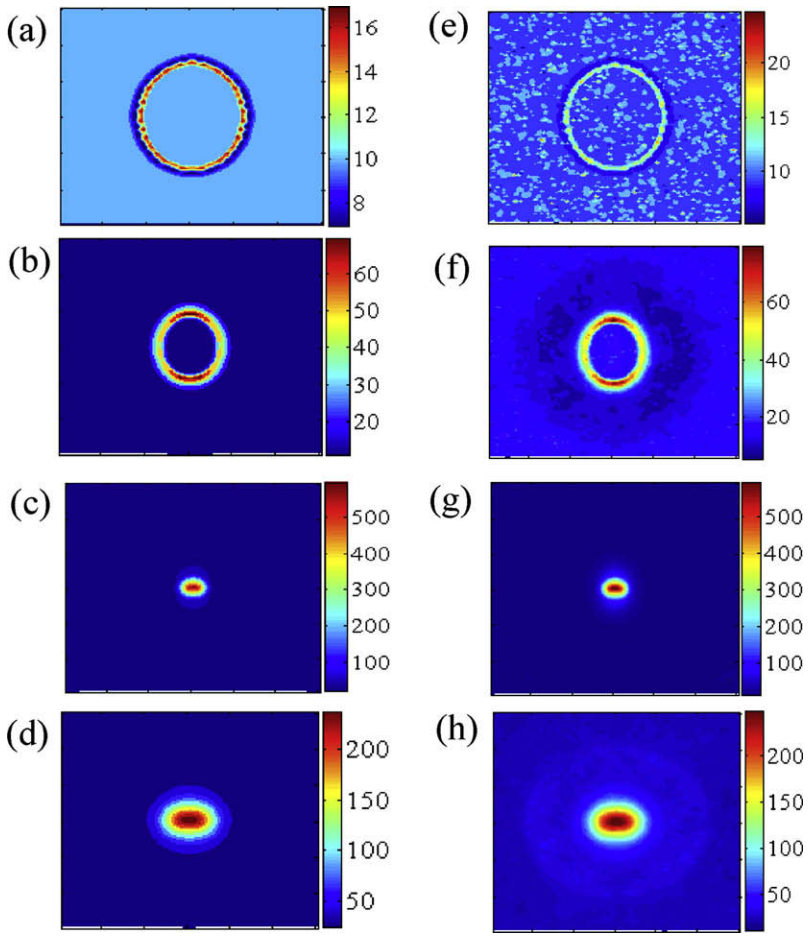

Fig. 6. Color contour maps of the spatial distribution of species B in the simulated domain for the "coarse model" (deterministic reactions) at times (a) 5, (b) 50, (c) 100, (d) 175 ltu steps, and "fine" model (kMC reactions) at times (e) 5, (f) 50, (g) 100, and (h) 175 ltu steps. The cavity has collapsed completely at 85 ltu. Initially the species B is distributed uniformly throughout the domain at a concentration of 10. Note the change in scale with time.

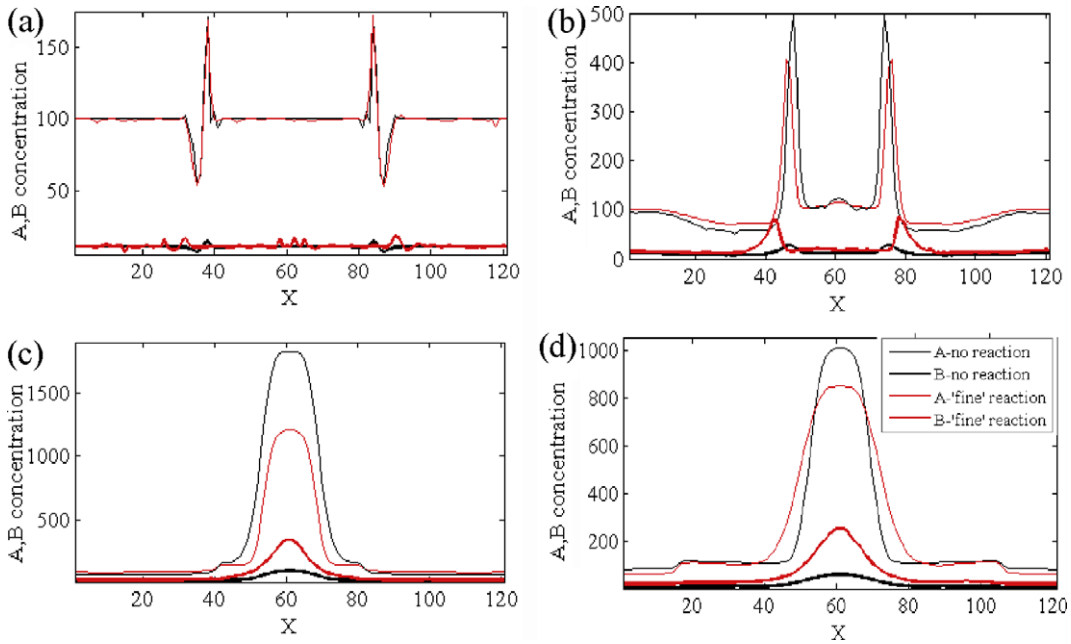

Fig. 7. Spatial distribution of species A (thin lines) and B (thick lines) across the simulated domain at times (a) 5, (b) 50, (c) 125, and (d) 150 ltu steps for a model of the collapsing cavity in absence of chemical reactions (black lines) and fine model with kMC reactions (red black lines) of the collapsing cavity with deterministic chemical reactions. The cavity has collapsed completely at 85 ltu. Initially the species A and B are distributed uniformly throughout the domain at concentrations of 100 and 10, respectively. Note the change of scale with time.

appearance of a concentration step on the periphery of the enriched region (most visible for the A species). The effect of chemical reactivity is clearly seen in Fig. 7c where conversion of A into B leads to a significant decrease in A concentration in the enriched region and a significant increase in B concentration. The enrichment due to advection associated with the cavity collapse leads to an enhancement in local chemical conversion of A into B. At time of 150 ltu steps, the concentration step following the pressure wave has expanded to nearly the edges of the simulation domain. More interestingly, while the concentration in A for the reactive model is, as expected, less than that of the non-reactive model at the center of the simulation domain, the spatial distribution of the A species is broader in the former case than in the later. At this time, the smaller difference in concentration of the A and B species allows sufficient conversion of B species into A to align the width of their distributions. This is clearly not the case in the simulation without chemical reactions.

Since the chemical reactions considered here are linear, the overall yield is not affected by the inhomogeneity in species concentration. However, provided the reaction dynamics is non-linear, the inhomogeneity in the concentration of species due to the hydrodynamics of the cavity may result in a significant change in the total yield of the reactions.

4. Conclusions

We have developed a LBM model of reactive-flow for multiphase systems. The reactive-flow model of a collapsing cavity developed in this study shows little difference in behavior associated with the stochasticity of the chemical reactions. In a two-species model for chemical reactions, the major difference observed takes only the form of random fluctuations in concentration of the minority species. Although our model is illustrated for the case of a two-component reaction with linear kinetics, its extension to multiple simultaneous reactions as for instance those involved in the formation of OH radicals [21] and non-linear kinetics is straightforward. The current model simulated cavitation under isothermal conditions so reaction kinetics enhancement due to the high temperature known to occur in collapsing cavities is not accounted for. The assumption of isothermal collapse is made herein by our choice of the Equation of State (EOS) ($\rho - P$ relation) which is consistent with that of an isothermal process [4,5]. Modeling adiabatic condition requires that we replace the isothermal EOS with an EOS consistent with the adiabatic behavior and couple it with the Thermal Lattice Boltzmann model [22]. The primary scientific observation of this study is that advection associated with the hydrodynamics of a collapsing cavity leads to highly inhomogeneous concentration of dissolved chemical species. In turn these inhomogeneities in concentration lead to significant increase in concentration-dependent reaction rates and can result in the enhancement in the production of minor species. The present study clearly suggests that any realistic model of sonochemistry must account for inhomogeneous distribution of chemical species inside and in the vicinity of collapsing cavities due to advective processes. The observed phenomena of advective enrichment at the moving liquid–vapor interface of a cavity sheds light on a possible mechanism in the synthesis of hollow microspheres in sonicated solutions containing a variety of substances such as proteins [23–26] or nanoparticles [27]. For instance, the advective process may concentrate fluid-supported proteins in a shell near the liquid–vapor interface which can subsequently be crosslinked by chemical processes associated with the presence of radical species [24].

Acknowledgement

This research was supported by the Mathematical, Information, and Computational Sciences Division, Office of Advanced Scientific Computing Research, US Department of Energy.

References

[1] R.W. Wood, A.L. Loomis, Phil. Mag. 4 (1927) 414.
[2] K.S. Suslick, Science 247 (1990) 1439.

[3] K.S. Suslick, Y. Didenko, M.M. Fang, T. Hyeon, K.J. Kolbeck, W.B. McNamara III, M.M. Mdleleni, M. Wong, Phil. Trans. R. Soc. Lond. A 357 (1999) 335.
[4] D.V. Prasad Naidu, R. Rajan, R. Kumar, K.S. Ghandi, V.H. Arakeri, S. Chandrasekaran, Chem. Eng. Sci. 48 (1994) 877.
[5] S. Sochard, A.M. Wilhelm, H. Delmas, Ultrason. Sonochem. 4 (1997) 77.
[6] S. Sochard, A.M. Wilhelm, H. Delmas, Chem. Eng. Sci. 53 (1998) 239.
[7] A. Sharma, P.R. Gogate, A. Mahilkar, A.B. Pandit, Chem. Eng. J. 143 (2008) 201.
[8] M.P. Brenner, Rev. Modern. Phys. 74 (2002) 425.
[9] J.F. Lutsko, J. Chem. Phys. 125 (2006) 164319.
[10] F.R. Young, Cavitation, McGraw-Hill, London, 1989.
[11] J.B. Keller, M. Miksis, J. Acous. Soc. Am. 68 (1980) 628.
[12] M.C. Sukop, D. Or, Phys. Rev. E 71 (2005) 046703.
[13] S. Succi, The Lattice Boltzmann Equation for Fluid Dynamics and Beyond, Clarendon Press, Oxford, 2001.
[14] D.A. Wolf-Gladrow, Lattice-Gas Cellular Automata, Lattice Boltzmann Models: An Introduction, Lecture Notes in Mathematics, Springer, Berlin, 2000.
[15] M.C. Sukop, D.T. Thorne, Lattice Boltzmann Modeling An introduction to Geoscientist and Engineers, Springer, Berlin, 2005.
[16] X. Shan, H. Chen, Lattice Boltzmann model for simulating flows with multiple phases and components, Phys. Rev. E 47 (1993) 1815–1819.
[17] X. He, G.D. Doolen, J. Stat. Phys. 107 (2002) 309.
[18] T.M. Truskett, P.D. Debenedetti, S. Sastry, S. Torquato, A single-bond approach to orientation-dependent interactions and its implications for liquid water, J. Chem. Phys. 111 (1999) 2647–2656.
[19] H.W. Stockman, C. Copper, C. Li, S.J. Perea-Reeves, Practical application of lattice-gas and lattice Boltzmann methods to dispersion problems, Int. J. Complex Syst. Paper 90 (1997) (<http://www.interjournal.org/>).
[20] D.T. Gillespie, Exact stochastic simulation of coupled chemical reactions, J. Phys. Chem. 81 (1977) 25.
[21] R. Togel, S. Hilgenfeldt, D. Lohse, Phys. Rev. Lett. 88 (2002) 34301.
[22] X.Y. He, S.Y. Chen, G.D. Doolen, A noevl thermal model for the lattice Boltzmann Method in incompressible limit, J. Comput. Phys. 146 (1998) 282–300.
[23] M.W. Grinstasff, K.S. Suslik, Proc. Nat. Acad. Sci. USA 88 (1991) 7708.
[24] K.S. Suslik, M.W. Grinstaff, K.J. Kolbeck, M. Wong, Ultrason. Sonochem. 1 (1994) S65.
[25] S. Avivi (levi), A. Dedanken, Ultrason. Sonochem. 12 (2005) 405.
[26] O. Grinberg, M. Hayun, B. Sredni, A. Gedanken, Ultrason. Sonochem. 14 (2007) 661.
[27] J.H. Bang, K.S. Suslik, J. Am. Chem. Soc. 129 (2007) 2242.